

Article

# Cocrystal Assembled by Pyrene Derivative and 1,4-Diiodotetrafluorobenzene via a C=O...I Halogen Bond

Qi Feng <sup>1</sup>, Wenhui Huan <sup>1</sup>, Jiali Wang <sup>1</sup>, Fang Guo <sup>1</sup>, Jiadan Lu <sup>1</sup>, Guowang Diao <sup>1,\*</sup> and Yaqi Shan <sup>2</sup>

<sup>1</sup> School of Chemistry & Chemical Engineering, Yangzhou University, Yangzhou 225002, China; fengqi3000@163.com (Q.F.); 18252722156@163.com (W.H.); jlwang0060@163.com (J.L.); sg033@163.com (F.G.); 18762314798@163.com (J.L.)

<sup>2</sup> School of Chemistry and Chemical Engineering, Southeast University, Nanjing 211189, China; 230159523@seu.edu.cn

\* Correspondence: gwldiao@yzu.edu.cn; Tel.: +86-0514-87975587

Received: 12 September 2018; Accepted: 11 October 2018; Published: 17 October 2018



**Abstract:** Cocrystal formation is a strategy used to modify the solid-state properties of a given molecule. In this study, a new cocrystal assembled by 1,4-Diiodotetrafluorobenzene (1,4-DITFB) and a pyrene derivative, 1-acetyl-3-phenyl-5-(1-pyrenyl)-pyrazoline (APPP), was synthesized. Due to the twisted structure of APPP, the crystal structure is greatly different with some large  $\pi$ -conjugated compounds, which exhibits edge-to-face  $\pi$ -stacked arrangement between 1,4-DITFB and pyrene rings, rather than the face-to-face  $\pi$ -stacked arrangement. Hirshfeld surface analysis and the shift of characteristic vibration band of the carbonyl group in FT-IR spectroscopy suggest the formation of a C=O...I halogen bond.

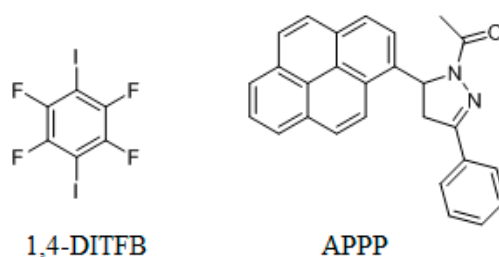
**Keywords:** cocrystal; pyrene derivative; 1,4-DITFB

## 1. Introduction

Cocrystals have gained significant interest in recent years due to their ability to improve the solid-state properties for pharmaceutical and materials science applications, including pharmaceutical solubility, drug dissolution rate, drug stability and mechanical properties (tableability), etc. [1–8]. In addition, the cocrystal strategy has been also used in some other research areas, such as the design of new explosives, or studying the relationship between density and explosive power, and so on [9,10].

In recent years, 1,4-diiodotetrafluorobenzene (1,4-DITFB, Scheme 1) has received much attention because it is an ideal halogen bonding (XB) donor and has become an important tool in supermolecular chemistry to develop more materials and medicines [11–13]. Jin et al. have reported that cocrystal assembled by 1,4-DITFB and some chromophores [14–17]. For the large  $\pi$ -conjugated compounds, such as pyrene, the cocrystal shows the column-like structure via  $\pi$ - $\pi$  stacking of the two components, whereas the small  $\pi$ -conjugated compounds, such as naphthalene or phenanthrene, usually adopt edge-to-face  $\pi$ -stacked arrangement with 1,4-DITFB. Compared with the planar compound, the chromophores with the twisted structures could not only restrict the molecular aggregation but also form some particular structures. In the present study, we synthesized a new cocrystal assembled by 1,4-DITFB and a pyrene derivative: 1-acetyl-3-phenyl-5-(1-pyrenyl)-pyrazoline (APPP, Scheme 1). In the cocrystal, APPP exhibits a twisted structure with the dihedral angle of 60.98° between the pyrazoline and pyrene rings. As a result, the cocrystal structure is significantly different with 1,4-DITFB and pyrene complex, which exhibits an edge-to-face  $\pi$ -stacked arrangement between 1,4-DITFB and pyrene rings, rather than the face-to-face  $\pi$ -stacked arrangement. Moreover,

FT-IR spectroscopy and Hirshfeld surface analysis were performed to understand the driving force for the cocrystal.



**Scheme 1.** Chemical Structures of 1,4-DITFB and APPP.

## 2. Materials and Methods

### 2.1. Crystal Preparation

All the reagents and solvents used for syntheses were purchased from Sigma Aldrich and were used without further purification. The target compounds were synthesized and characterized by previously reported methods [18,19]. APPP: a mixture of acetophenone (1.2 g), 1-pyrenecarboxaldehyde (2.3 g), and 3 M of aqueous sodium hydroxide (6 mL) in ethanol (20 mL) was stirred at room temperature for 8 h. The resulting solid was filtered to afford 1-phenyl-3-(pyren-1-yl) prop-2-en-1-one (chalcone). Then chalcone (1 g) and 3.5 g of hydrazine hydrate aqueous solution (80%) were dissolved in 20 mL of glacial acetic acid. The mixture was then stirred at 120 °C for 5 h, and the resulting solution was cooled to room temperature and poured into a beaker containing ice water slowly. The crude product was collected by filtration and recrystallized from ethyl acetate to give pure APPP as a yellow powder: 0.64 g, yield: 60%.

1,4-DITFB: Iodine and 65% fuming sulfuric acid (15 mL) were mixed and stirred at room temperature for 30 min. Then 5 g tetrafluorobenzene was added. Subsequently, the mixture was heated at 55–60 °C for 3 h. The mixture was cooled and poured over crushed ice. A dark solid formed which was filtered, washed with aqueous sodium bisulfite and dried. The compound was recrystallized from methanol, giving 11 g white solid, yield: 80%.

The cocrystal was prepared as follow method: APPP and 1,4-DITFB in an equimolar ratio were dissolved in tetrahydrofuran in a glass vial. Slow evaporation of the solvent at room temperature for approximately two weeks yielded the needle, yellow crystals.

### 2.2. Measurement

Single-crystal X-ray diffraction experiments were carried out using a Bruker D8 QUEST diffractometer (Bruker, Billerica, MA, USA) equipped with a Bruker APEX-II ( $\lambda = 0.71073 \text{ \AA}$ ). Data collection was done at ambient temperature. The structure was solved with direct method using SHELXL program and refined anisotropically using a full-matrix least-squares procedure [20]. All non-hydrogen atoms were refined anisotropically and hydrogen atoms were inserted at their calculated positions and fixed at their positions. The structural data has been deposited as CIFs at the Cambridge Crystallographic Data Base (CCDC No. 1855431). The PXRD patterns were measured with a Bruker D8 advance superspeed powder diffractometer (Bruker, Billerica, MA, USA), which operated at ambient temperature, using Cu K $\alpha$  radiation ( $\lambda = 0.15405 \text{ nm}$ ), a voltage of 40 kV and a current of 40 mA. Differential scanning calorimetry (DSC) patterns were recorded with a Mettler-Toledo Thermogravimetric Analyzer (TA Instruments, New Castle, UK) with the temperature scanned from 50 to 300 °C at a heating rate of 10 °C/min. FT-IR spectra were recorded on a Bruker Tensor 27 FT-IR spectrometer (Bruker, Billerica, MA, USA) by using a KBr pellet.

### 2.3. Hirshfeld Surface Analysis

Hirshfeld surface graphical representation over  $d_{\text{norm}}$  around the two neighboring molecules of APPP and 1,4-DITFB from the cocrystal structure and associated 2D fingerprint plot were performed out by using Crystal Explorer 3.1 [21].

## 3. Results

### 3.1. Crystal Structure

The cocrystal consists of 1:1 molar ratio between APPP and 1,4-DITFB molecules, and only one independent molecule of these exists in the asymmetric unit (ASU). The Crystallographic data and ORTEP plot are presented in Table 1 and Figure 1, respectively.

**Table 1.** Crystallographic data and refinement for the cocrystal.

Crystal	APPP and 1,4-DITFB Cocrystal
Formula	$\text{C}_{33}\text{H}_{21}\text{F}_4\text{I}_2\text{N}_2\text{O}$
Temperature/K	296(2)
morphology	needle
Crystal system	monoclinic
Space group	$P2_1/c$
$a/\text{\AA}$	7.5134(6)
$b/\text{\AA}$	29.349(3)
$c/\text{\AA}$	13.3746(12)
$\alpha/\text{deg}$	90
$\beta/\text{deg}$	100.924(3)
$\gamma/\text{deg}$	90
$V/\text{\AA}^3$	2895.8(4)
Z	4
$\rho$ (calcd)/ $\text{Mg m}^{-3}$	1.815
$\theta$ Range for data collection/ $^\circ$	2.081–27.590
$F(000)$	1532
$R_1, wR_2$ ( $I > 2\sigma(I)$ )	0.0583, 0.1400
$R_1, wR_2$ (all data)	0.0956, 0.1566
Goodness-of-fit, S	1.015
CCDC	1,855,431

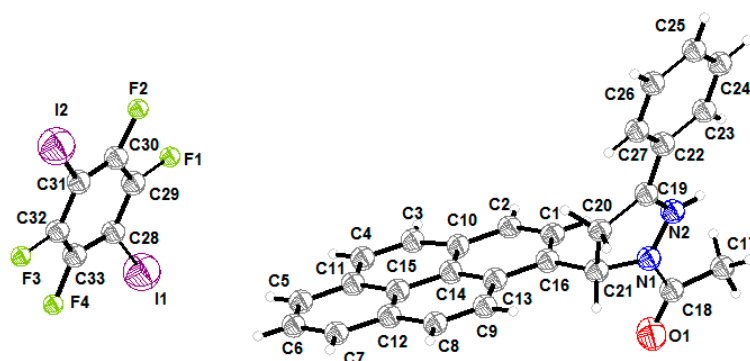


**Figure 1.** The ORTEP plot of the cocrystal.

The cocrystal forms in the monoclinic centrosymmetric space group  $P2_1/c$ . The dihedral angle between the pyrazoline ring and pyrene ring is  $66.70^\circ$ . As shown in Figure 2, 1,4-DITFB is linked with two adjacent one-handed APPP molecules through  $\text{C}=\text{O}\cdots\text{I}$  and  $\text{C}-\text{I}\cdots\pi$  halogen bonds (Table 2), with  $\text{O}\cdots\text{I}$  and  $\text{I}\cdots\pi$  distances of 3.059 and 3.571  $\text{\AA}$  respectively, which accord with the previous reports ( $\text{O}\cdots\text{I} = 3.034 \text{\AA}$  and  $\text{I}\cdots\pi = 3.551\text{--}3.553 \text{\AA}$ ) [22,23]. Due to these halogen bonds, 1,4-DITFB and APPP

molecules are stacked alternately and extend along the *b* axis to construct the 1D chain motif. The two neighboring 1D chains with opposite chirality are connected by C–H···O hydrogen bond, resulting in the racemic columnar network, which is stacked in a parallel fashion to provide the 3D structure. Compared with the pyrene and 1,4-DITFB complex, the pyrene rings in this study adopt edge-to-face  $\pi$ -stacked arrangement with 1,4-DITFB, the reason may be the C=O···I halogen bond and the twisted structure of APPP hinder the parallel arrangement between them.

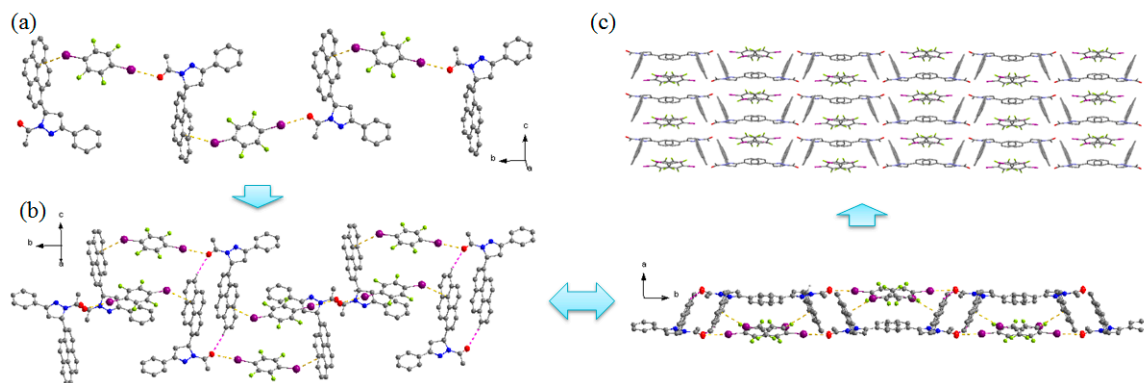


**Figure 2.** The cocrystal structure: (a) 1D chain motif. (b) Arrangement of the 1D chains with opposite chirality. (c) 3D structure of the cocrystal. Hydrogen atoms not participating in the interactions have been omitted for clarity.

**Table 2.** Halogen bonds geometry (Å, deg) for the cocrystal.

D–X···A	D–X	X···A	D···A	D–X···A
C(18)=O(1)···I(1)	1.217	3.059	3.815	119.97
C(31)-I(2)··· $\pi$ (C15)	2.068	3.571	5.435	147.89

### 3.2. Powder X-ray Diffraction (PXRD) Patterns

The cocrystal was also determined by PXRD analysis. Its PXRD pattern (Figure 3) is distinctly different from the pure APPP, and coincide with the simulated PXRD patterns calculated from its crystal data, which would be used for DSC and FT-IR measurement.

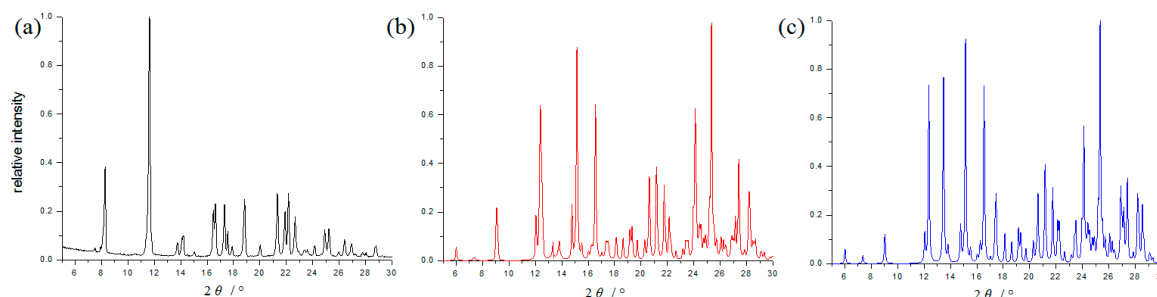


**Figure 3.** PXRD patterns of the pure APPP (a), the cocrystal (b) and simulated PXRD pattern of the cocrystal (c).

### 3.3. Thermal Properties

Differential scanning calorimetry (DSC) was employed to investigate the thermal behavior of the cocrystal (Figure 4). It could be observed that the cocrystal exhibits only one endothermic peak at 175 °C. However, the pure APPP exhibits one endothermic peak at 205 °C. The different thermal properties further suggests that the formation of a new phase.

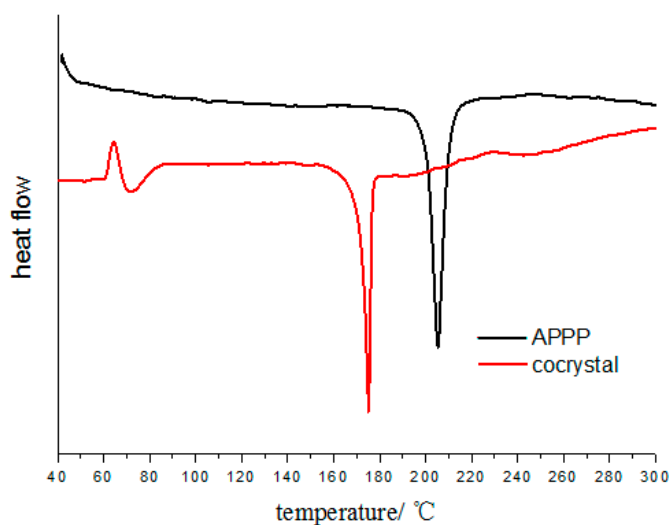


**Figure 4.** DSC patterns of the cocystal and pure APPP.

### 3.4. FT-IR Spectroscopy and Hirshfeld Surface Analysis

To investigate the non-covalent interactions within the cocystal, the FT-IR spectra were recorded (Figure 5). Compared with the characteristic vibration band of the carbonyl group in pure APPP at  $1653\text{ cm}^{-1}$ , the value in the cocystal shifts to lower frequencies by approximately  $6\text{ cm}^{-1}$ . This indicates that the intermolecular  $\text{C}=\text{O}\cdots\text{I}$  halogen bond influence the vibrational properties of APPP, and the result is consistent with other molecular crystal structures already reported by our group [18,24].

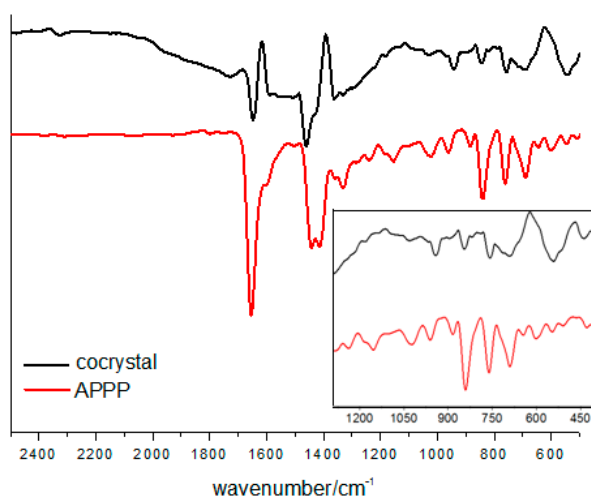


**Figure 5.** FT-IR spectra of the cocystal and pure APPP.

Hirshfeld surface analysis was also performed to give insights regarding the important intermolecular interactions in the cocystal [25]. The inspection of the intermolecular interactions is normalized by van der Waals radii through a red-white-blue color scheme, where the red spots denote closer contacts of molecules. As shown in Figure 6, the molecular surface mainly exhibits a red spot due to the close contact by  $\text{C}=\text{O}\cdots\text{I}$  halogen bond between APPP and 1,4-DITFB. In addition, a little red spot could be found on another APPP molecule, corresponding to the  $\text{C}-\text{I}\cdots\pi$  halogen bond between the pyrenyl and 1,4-DITFB. This further proves the importance of  $\text{C}=\text{O}\cdots\text{I}$  halogen bond for constructing the cocystal. As a result, the cocystal is significantly different from the pyrene and 1,4-DITFB complex.

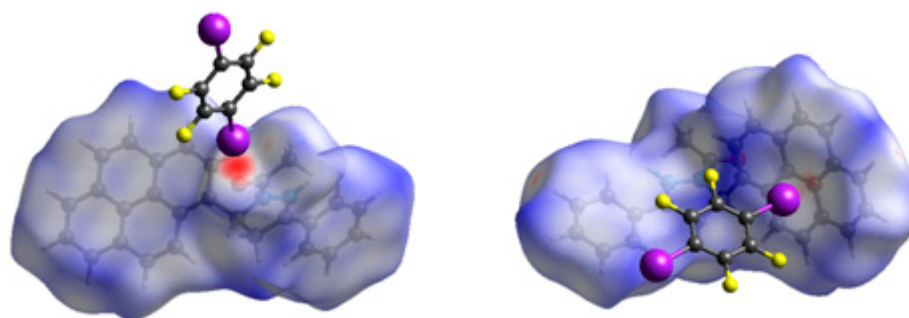


Figure 6. Hirshfeld surface mapped with  $d_{\text{norm}}$  for the cocrystal.

Two-dimensional fingerprint plot over the Hirshfeld surface was used to highlight the nature and contribution of the intermolecular interactions for crystal packing (Figure 7 and Table 3). It could be observed that weak  $\text{H}\cdots\text{H}$  contacts display major contribution in crystal packing cohesion, with 28.3% of total surface area. The  $\text{H}\cdots\text{F}$  contacts with second major contribution comprise 21.8% of total surface area. Apart from that,  $\text{C}\cdots\text{H}$ ,  $\text{C}\cdots\text{C}$  and  $\text{H}\cdots\text{I}$  contacts also show important contribution for the supramolecular architectures from 10.1 to 12.5% of total surface area in the fingerprint plot. Moreover, the  $\text{C}=\text{O}\cdots\text{I}$  halogen bond ( $\text{I}\cdots\text{O}$ ) in percentage contribution is 0.9% and appears as two spikes in the top left ( $\text{O}\cdots\text{I}$ ) and bottom right ( $\text{I}\cdots\text{O}$ ) areas of the related plot.

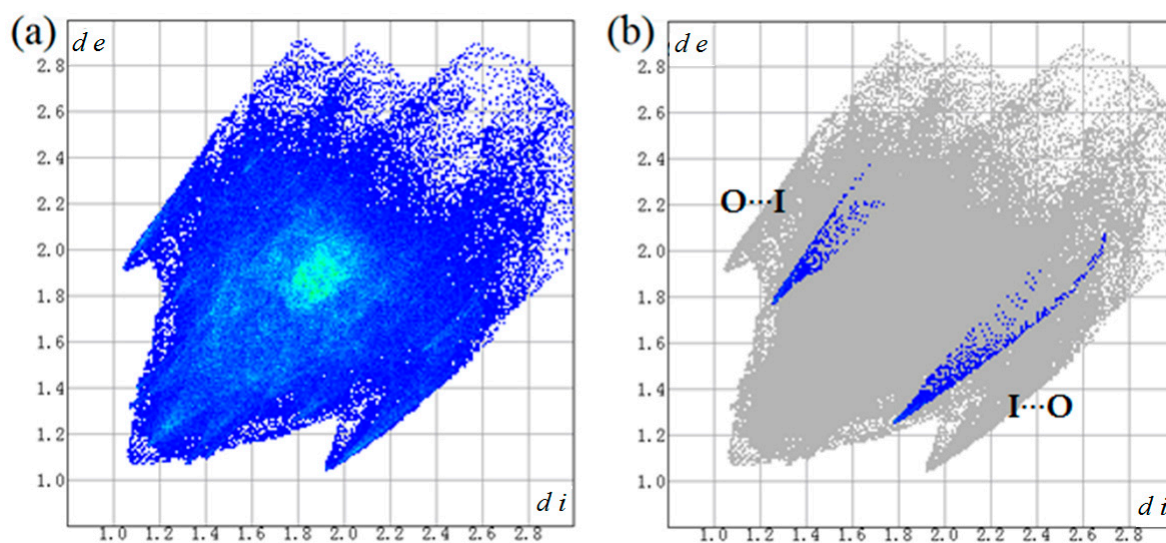


Figure 7. Two-dimensional fingerprint plots for the cocrystal (a) and  $\text{O}\cdots\text{I}$  /  $\text{I}\cdots\text{O}$  interaction (b).

Table 3. Contributions of the intermolecular contacts.

Contact	%	Contact	%
$\text{I}\cdots\text{O}$	0.9	$\text{H}\cdots\text{F}$	19.7
$\text{O}\cdots\text{H}$	4.9	$\text{H}\cdots\text{H}$	28.3
$\text{C}\cdots\text{C}$	10.7	$\text{C}\cdots\text{H}$	12.5
$\text{C}\cdots\text{F}$	3.5	$\text{C}\cdots\text{I}$	4.7
$\text{C}\cdots\text{N}$	0.1	$\text{H}\cdots\text{I}$	10.1
$\text{H}\cdots\text{N}$	0.2	$\text{F}\cdots\text{F}$	2.6
$\text{F}\cdots\text{I}$	1.0	$\text{F}\cdots\text{N}$	0.4
$\text{I}\cdots\text{N}$	0.4		

#### 4. Conclusions

In summary, we have synthesized a new cocrystal assembled by 1,4-DITFB and APPP. Compared with 1,4-DITFB and pyrene complex, this cocrystal exhibits different structure, in which the pyrene rings adopt edge-to-face  $\pi$ -stacked arrangement with 1,4-DITFB. FT-IR spectroscopy allowed for determining the driving force of the cocrystal by the shifts of the C=O vibration bands, and the Hirshfeld surface analysis was further proved that the cocrystal was constructed mainly through a C=O $\cdots$ I halogen bond.

**Author Contributions:** Q.F. designed the experiments, wrote and revised the manuscript; W.H. and J.W. performed the X-ray single diffraction study and Hirshfeld surface analysis; F.G. and Y.S. synthesized the cocrystal; J.L. performed the IR spectra spectroscopy; G.D. conceived the project.

**Funding:** This work is partly supported by the National Natural Science Foundation of China (Grant No. 21773203), Certificate of China Postdoctoral Science Foundation Grant (No. 2018M632387), the Natural Science Foundation of the Jiangsu Higher Education Institutions of China (No. 18KJB150035), and Innovation and Cultivation Fund of Yangzhou University (No. 2017CXJ012).

**Conflicts of Interest:** The authors declare no conflict of interest.

#### References

1. Przybyłek, M.; Ziolkowska, D.; Mroczynska, K.; Cysewski, P. Applicability of phenolic acids as effective enhancers of cocrystal solubility of methylxanthines. *Cryst. Growth Des.* **2017**, *17*, 2186–2193. [[CrossRef](#)]
2. Ranjan, S.; Devarapalli, R.; Kundu, S.; Vangala, V.R.; Ghosh, A.; Reddy, C.M. Three new hydrochlorothiazide cocrystals: Structural analyses and solubility studies. *J. Mol. Struct.* **2017**, *1133*, 405–410. [[CrossRef](#)]
3. Panzade, P.; Shendarkar, G.; Shaikh, S.; Rathi, P.B. Pharmaceutical cocrystal of piroxicam: Design, formulation and evaluation. *Adv. Pharm. Bull.* **2017**, *7*, 399–408. [[CrossRef](#)] [[PubMed](#)]
4. Cysewski, P.; Przybyłek, M. Selection of effective cocrystals former for dissolution rate improvement of active pharmaceutical ingredients based on lipoaffinity index. *Eur. J. Pharm. Sci.* **2017**, *107*, 87–96. [[CrossRef](#)] [[PubMed](#)]
5. Krishna, G.R.; Shi, L.M.; Bag, P.P.; Sun, C.C.; Reddy, C.M. Correlation among crystal structure, mechanical behavior, and tableability in the co-crystals of vanillin isomers. *Cryst. Growth Des.* **2015**, *15*, 1827–1832. [[CrossRef](#)]
6. Karagianni, A.; Malamatar, M.; Kachrimanis, K. Pharmaceutical cocrystals: New solid phase modification approaches for the formulation of APIs. *Pharmaceutics* **2018**, *10*. [[CrossRef](#)] [[PubMed](#)]
7. Thakuria, R.; Sarma, B. Drug-drug and drug-nutraceutical cocrystal/salt as alternative medicine for combination therapy: A crystal engineering approach. *Crystals* **2018**, *8*, 101. [[CrossRef](#)]
8. Aitipamula, S.; Vangala, V.R. X-ray crystallography and its role in understanding the physicochemical properties of pharmaceutical cocrystals. *J. Indian Inst. Sci.* **2017**, *97*, 227–243. [[CrossRef](#)]
9. Hang, G.Y.; Yu, W.L.; Wang, T.; Wang, J.T.; Li, Z. Molecular dynamics calculation on structures, stabilities, mechanical properties, and energy density of CL-20/FOX-7 cocrystal explosives. *J. Mol. Model.* **2018**, *23*. [[CrossRef](#)] [[PubMed](#)]
10. Ghosh, M.; Sikder, A.K.; Banerjee, S.; Gonnade, R.G. Studies on CL-20/HMX (2:1) cocrystal: A new preparation method and structural and thermokinetic analysis. *Cryst. Growth Des.* **2018**, *18*, 3781–3793. [[CrossRef](#)]
11. Zhuo, M.; Tao, Y.; Wang, X.; Wu, Y.; Chen, S.; Liao, L.; Jiang, L. 2D organic photonics: An asymmetric optical waveguide in self-assembled halogen-bonded cocrystals. *Angew. Chem. Int. Ed.* **2018**, *57*, 11300–11304. [[CrossRef](#)] [[PubMed](#)]
12. Rozhkov, A.V.; Novikov, A.S.; Ivanov, D.M.; Bolotin, D.S.; Bokach, N.A.; Kukushkin, V.Y. Structure-directing weak interactions with 1,4-Diiodotetrafluorobenzene convert one-dimensional arrays of [M-II(acac)(2)] species into three-dimensional networks. *Cryst. Growth Des.* **2018**, *18*, 3626–3636. [[CrossRef](#)]
13. Pigge, F.C.; Vangala, V.R.; Swenson, D.C. Relative importance of X $\cdots$ O=C vs. X $\cdots$ X halogen bonding as structural determinants in 4-halotriarylbenzenes. *Chem. Commun.* **2006**, *20*, 2123–2125. [[CrossRef](#)] [[PubMed](#)]

14. Shen, Q.; Pang, X.; Zhao, X.; Gao, H.; Sun, H.; Jin, W. Phosphorescent cocrystals constructed by 1,4-diodotetrafluorobenzene and polyaromatic hydrocarbons based on C–I $\cdots$  $\pi$  halogen bonding and other assisting weak interactions. *CrystEngComm* **2012**, *14*, 5027–5034. [[CrossRef](#)]
15. Gao, H.; Shen, Q.; Zhao, X.; Yan, X.; Pang, X.; Jin, W. Phosphorescent co-crystal assembled by 1,4-diodotetrafluorobenzene with carbazole based on C–I $\cdots$  $\pi$  halogen bonding. *J. Mater. Chem.* **2012**, *22*, 5336–5343. [[CrossRef](#)]
16. Gao, Y.; Li, L.; Liu, R.; Jin, W. Phosphorescence of several cocrystals assembled by diiodotetrafluorobenzene and three ring angular diazaphenanthrenes via C–I $\cdots$ N halogen bond. *Spectrochim. Acta Part A* **2017**, *173*, 792–799. [[CrossRef](#)] [[PubMed](#)]
17. Liu, R.; Gao, Y.; Jin, W. Color-tunable phosphorescence of 1,10-phenanthrolines by 4,7-methyl/-diphenyl/-dichloro substituents in cocrystals assembled via bifurcated C–I $\cdots$ N halogen bonds using 1,4-diodotetrafluorobenzene as a bonding donor. *Acta Crystallogr. B* **2017**, *B73*, 247–254. [[CrossRef](#)] [[PubMed](#)]
18. Feng, Q.; Wang, M.; Dong, B.; He, J.; Xu, C. Regulation of arrangements of pyrene fluorophores via solvates and cocrystals for fluorescence modulation. *Cryst. Growth Des.* **2013**, *13*, 4418–4427. [[CrossRef](#)]
19. Hellmann, M.; Bilbo, A.J.; Pummer, W.J. Synthesis and Properties of Fluorinated Polyphenyls. *J. Am. Chem. Soc.* **1955**, *77*, 3650–3651. [[CrossRef](#)]
20. Sheldrick, G.M. A short history of SHELX. *Acta Crystallogr. A* **2008**, *64*, 112–122. [[CrossRef](#)] [[PubMed](#)]
21. Wolff, S.K.; Grimwood, D.J.; McKinnon, J.J.; Jayatilaka, D.; Spackman, M.A. *CrystalExplorer 3.1*; The University of Western Australia: Perth, Australia, 2012.
22. Nwachukwu, C.I.; Bowling, N.P.; Bosch, E. C–I $\cdots$ N and C–I $\cdots$  $\pi$  halogen bonding in the structures of 1-benzylidimidazole derivatives. *Acta Crystallogr. C* **2017**, *73*, 2–8. [[CrossRef](#)] [[PubMed](#)]
23. Umezono, S.; Okuno, T. Systematic study of intermolecular C–X $\cdots$ O=S (X = Cl, Br, I) halogen bonds in (E)-10-(1,2-dihalovinyl)-10H-phenothiazine 5,5-dioxides. *J. Mol. Struct.* **2017**, *1147*, 636–642. [[CrossRef](#)]
24. Feng, Q.; Wang, M.; Dong, B.; Xu, C.; Zhao, J.; Zhang, H. Tuning solid-state fluorescence of pyrene derivatives via a cocrystal strategy. *CrystEngComm* **2013**, *15*, 3623–3629. [[CrossRef](#)]
25. McKinnon, J.J.; Spackman, M.A.; Mitchell, A.S. Novel tools for visualizing and exploring intermolecular interactions in molecular crystals. *Acta Crystallogr. B* **2004**, *60*, 627–668. [[CrossRef](#)] [[PubMed](#)]



© 2018 by the authors. Licensee MDPI, Basel, Switzerland. This article is an open access article distributed under the terms and conditions of the Creative Commons Attribution (CC BY) license (<http://creativecommons.org/licenses/by/4.0/>).